Local electronic and magnetic structure of mixed ferrite multilayer materials

Daniel M. Wells,[1,2] J. Cheng,[3,2] Donald E. Ellis,[1,4,2] and B. W. Wessels[3,2]
[1]*Department of Chemistry, Northwestern University, 2145 Sheridan Road, Evanston, Illinois 60208-3113, USA*
[2]*Materials Research Center, Northwestern University, 2145 Sheridan Road, Evanston, Illinois 60208-3113, USA*
[3]*Department of Materials Science and Engineering, Northwestern University, 2145 Sheridan Road, Evanston, Illinois 60208-3113, USA*
[4]*Department of Physics & Astronomy, Northwestern University, 2145 Sheridan Road, Evanston, Illinois 60208-3113, USA*
(Received 4 February 2010; published 24 May 2010)

Multilayer bispinel composites, in which one member is magnetite, Fe_3O_4, and the other is XFe_2O_4 (X =Mg,Mn,Ni,Co) are modeled using first-principles density-functional theory in a periodic supercell scheme. Effects of transition metal composition on charge distribution and magnetization are examined in detail in order to determine the range of variability attainable upon cation substitution and distribution. Magnetic measurement on bilayer $Fe_3O_4/MgFe_2O_4$ and $Fe_3O_4/CoFe_2O_4$ compositions are reported, showing a considerable increase in magnetization relative to the separate bulk compounds, in qualitative agreement with theory.

DOI: 10.1103/PhysRevB.81.174422 PACS number(s): 75.70.Cn, 75.50.Gg

I. INTRODUCTION

Magnetic exchange at the interface of two magnetic materials is interesting due to applications in magnetoresistive devices and spin based electronics, spintronics.[1,2] The main interest in doped ferrimagnetic ferrite materials, $CoFe_2O_4$ (CFO) and $MgFe_2O_4$ (MFO), is for spin barriers[3,4] used in conjunction with spin filters such as half metallic Fe_3O_4 (FO).[5] This type of composite has been demonstrated in several bilayer ferrite systems[6,7] where superexchange in these oxide/oxide systems has been shown to be a viable model of the magnetic coupling.[8] Pioneering efforts at forming multilayer bispinels were plagued by interface roughness, and formation of undesired phases, as evidenced in the FO/CFO case, which interfered with understanding magnetic structure possibilities.[9] With improved deposition techniques, the FO/CFO system has been extensively studied experimentally recently showing the magnetic coupling at the interface to be very important.[4,10,11] A recent study by Ramos *et al.* has demonstrated that the interface coupling is similar to that of the antiphase boundaries (APBs) commonly found in magnetic ferrite thin films.[10] APBs in FO thin films have been shown to greatly affect the magnetic and transport properties, decreasing the saturation magnetization,[12] coercivity,[13] and increased magnetoresistance[14,15] and saturation fields.[13] In the proposed model[14] the interface is strongly antiferromagnetically (AF) coupled, and decouples in a helical manner away from the interface. The linear dimensions of APB may be on the order of 5–100 nm (Ref. 13) and are thus difficult to study directly by first-principles methods; however, the underlying exchange interactions depend upon details of interface structure (orientation, roughness, interdiffusion), which can be probed by atomic-level theoretical analysis. In principle, the parameters needed for nanoscale domain modeling can be obtained from energetics of different spin orientations across the interface.

The materials modeled in this work are all ferrite based spinels; therefore, the lattice mismatch between these materials is very small, with that between FO and CFO being less than 1%. The cubic spinel structure contains eight formula units; one unit cell of volume approximately 590 Å^3 contains 24 metal ions and 32 O atoms. A normal spinel can be written as $M^{2+}(M^{3+})_2O_4$ with M^{2+} occupying eight tetrahedral sites (A site) in the cubic close packed O lattice and M^{3+} occupying 16 octahedral positions (B site). The (001) oriented structure of FO can also be viewed as a stacking of alternating Fe_4O_8 and Fe_2 layers. In an inverse spinel the A site is occupied by M^{3+} cations and the B-site is equally occupied by both M^{2+} and M^{3+} cations; the structure can be written as $M^{3+}(M^{2+}/M^{3+})_2O_4$. Of the materials considered in this work FO, MFO, CFO, and NFO are known to be inverse spinels or close to inverse spinel in cation arrangement. The electronic hopping between Fe^{2+} and Fe^{3+} cations gives magnetite its good electrical conductivity. Below the Verwey temperature, $T_V \approx 120$ K, the cations order and the resistivity increases exponentially.[16]

Calculations for bulk FO with inverse spinel structure provide a good reference state, as all metal sites are occupied by Fe and the charge and moment on every site is allowed to find its self-consistent value. Nontrivial results follow, as the nominal divalent and trivalent charge descriptions are significantly modified by metal-oxygen covalency.[17] Bulk calculations of FO, MFO, CFO, MnFO, and NFO were carried out in the present work for comparison to the composite materials, using the same methodology and density-functional theory (DFT) computational conditions.

The modulation of this covalency by structural relaxation and cation substitution provides one of the "handles" by which multilayer magnetization can be manipulated. As would be assumed from the above discussion, in CFO the Co cations localize to half the B-sites and Fe occupies the remaining B and A sites.[18] Specifically, in the present model two out of every four B sites in a layer are replaced by Co so the layers can be written as alternating $Co_2Fe_2O_8$ and Fe_2 layers. MFO actually forms as an intermediate spinel somewhere between normal and inverse and should be written as $(Mg^{2+}_{1-x}Fe^{2+}_x)(Mg^{2+}_xFe^{3+}_{2-x})O_4$.[19,20] The value of x in MFO is extremely dependent on the synthesis methods, but can reasonably range from 0.08 to 0.30 in the bulk.[19,20] The present MFO model contains 8 Mg ions, fully occupying the A sites

while the 16 Fe are all at *B* sites in the spinel unit cell. The lattice structure of Mn-ferrite is known to be nearly normal spinel, while Ni-ferrite is found to be inverse.[21,22] In view of the cation site variability of the transition metal spinels and its dependence upon preparation conditions, we may consider this as yet another useful variable for tuning magnetic properties. In the following it is convenient to refer to cation sites by their coordination type or connectivity; e.g., Fe(*T*) for *A* sites and Fe(*O*) for *B* sites.

II. COMPUTATIONAL DETAILS

Periodic spin-polarized band structure calculations were performed using the first principles DFT program Vienna *ab initio* simulation package (VASP) applying pseudopotentials with a periodic plane wave basis.[23–25] The exchange-correlation potential was chosen as the generalized gradient approximation (GGA) in a projector augmented wave (PAW) method developed by Kresse and Joubert.[26] Automatically generated Monkhorst-Pack grids were used to carry out Brillouin zone integrations.[27] Relaxation of the geometric positions was considered complete when the Hellmann-Feynmann forces were below 0.02 eV/Å on every atom. Initial geometric relaxations were conducted with a $2\times2\times2$ *k*-point mesh and increased to $4\times4\times2$ meshes ($4\times4\times4$ for bulk spinels) to establish convergence and calculate density of states (DOS). The total energy *E* per unit cell is calculated in each configuration; the quantity of primary interest here being the interface energy, defined as

$$\Delta_{AB} = (E_{AB} - E_A - E_B)/|\mathbf{a}_1 \times \mathbf{a}_2|. \quad (1)$$

Here E_{AB} is the energy of the bispinel cell, E_A and E_B are energies of the component spinel cells, and the denominator is the cross-sectional area of the interface.

The on-site Coulomb correction, a so-called Hubbard *U* term, was included in some final self consistent calculations in the method of Dudarev *et al.*[28] In this method the on-site Coulomb interaction, *U*, and on-site exchange interaction, *J*, are treated together as $U_{\text{eff}}=U-J$. Initial values of *U* were taken from previous work fitting the calculations to x-ray absorption spectra.[29] The Hubbard *U* values for Co; octahedral Fe, Fe(*O*); and tetrahedral Fe, Fe(*T*) used were 4.0, 4.0, and 4.5 eV, respectively. Values for neighboring Ni and Mn can be expected to be similar. Further, since experimentally optimum values of U_{eff} are not known for the various chemical and structural configurations studied here, a uniform value of 4 eV was selected for most calculations, as a reasonable average value for transition metals near the middle of the series. *K*-point meshes as large as $6\times6\times2$ were used initially for calculation of DOS and charge distribution; $4\times4\times2$ was found to give adequate precision. Since GGA $+U$ model structures were found to differ little from the simpler GGA values, a considerable number of later calculations applied the Coulomb correlation corrections at the end of the self-consistent field (SCF) lattice relaxation procedure.

Further, the magnetic anisotropy (MAE) of FO/*X*FO multilayers was investigated by the VASP implementation of spin-orbit coupling, SOC. MAE was explored within the SOC scheme by forcing the magnetization axis alternately to the [001], [010], [001], and [111] crystalline axis directions. The magnetization axis yielding the lowest energy structure is defined as the easy magnetization axis. With inclusion of SOC the spin density is coupled to the orbital angular momentum; i.e., the α and β spin magnetization densities are coupled to the lattice vectors. In order to retain the global magnetic (AF or Ferromagnetic-F) character of the DOS, the positive or negative density on any given ion for a given set of angular momentum-resolved orbitals was summed independent of magnetization direction. The partial and total DOS were then found by independently summing all positive or negative densities on each ion and for all ions, respectively.

III. EXPERIMENTAL

In support of the theoretical investigation, magnetic properties of the FO/MFO and FO/CFO bilayers composed of epitaxial Fe_3O_4, $MgFe_2O_4$, and $CoFe_2O_4$ thin films were measured. These bilayers were deposited on (001) oriented MgO substrates in a commercial molecular beam epitaxy (MBE) chamber manufactured by SVT Associates. Metallic iron, magnesium and cobalt sublimed from effusion cells, and molecular oxygen were used as reactants for the formation of these layers. Deposition was performed at 300 °C to minimize Mg diffusion from the substrate into the thin films. Fe_3O_4, $MgFe_2O_4$, and $CoFe_2O_4$ thin films synthesized using this method, as indicated from previous studies, exhibit bulk-like structural and magnetic properties.[30–33] To form bilayers, the shutter shielding the substrate from the reactants was closed for one minute after the deposition of one layer before subsequently reopening for the deposition of the next layer. The FO/MFO and FO/CFO bilayer structures have each layer 7–10 nm thick, which corresponds to 9–11 unit cells. The structural properties of these bilayers were examined using high-angle x-ray diffraction, secondary ion mass spectroscopy and transmission electron microscopy. These measurements indicate that the bilayers are epitaxial with an atomically abrupt interface formed between dissimilar spinel ferrite layers.[34,35] The magnetization of the bilayers as a function of applied magnetic field at 300 K was measured using a magnetic property measurement system (MPMS) magnetometer with an absolute sensitivity of 10^{-7} emu. The measurement was conducted in a longitudinal geometry such that the direction of the magnetic field is parallel to the sample surface. The magnetic properties of bilayers were investigated by referring to those of the single layers.

IV. RESULTS

A. Structural relaxation and charge/magnetization distribution

Structural features and electronic charge distributions of the multilayer bispinel systems can best be analyzed by comparison with those calculated for the corresponding bulk compounds. Our results for the bulk ferrites are in essential agreement with those of other workers, using similar methods. We would like to particularly point out the recent work of Perron *et al.* who presented a detailed study of NFO, of importance as a corrosion product in pressurized water

TABLE I. Lattice constants a (Å), cell volume (Å^3), and metal-oxygen bond lengths (Å) in bulk and multilayer bispinels; minimum to maximum values of bond lengths are given. The value of a given represents an average over the slightly distorted cubic cell for bulk compounds; the value of c represents $\frac{1}{2}$ the c-axis length of the bispinel cell.

Bulk compound	FO	MFO	CFO	MnFO	NFO
a	8.330, 8.398[a]	8.300, 8.375[a]	8.235, 8.380[a]	8.261, 8.515[a]	8.220, 8.336[a]
Volume (Å^3)	578.0 592[a]	571.8 587[a]	558.5 588[a]	563.3 617[a]	556.6 579[a]
Fe(T)-O	1.87	1.95–2.03	1.84–1.85	1.87–1.90	1.85–1.86
Fe(O)-O	2.03–2.06	1.99–2.06	2.00–2.05	2.01–2.03	1.98–2.04
X(O)-O		2.00–2.10	2.02–2.05	1.99–2.01	2.01–2.03
Layered compound		**FO/MFO**	**FO/CFO**	**FO/MnFO**	**FO/NFO**
a,b,c		8.288, 8.285 8.300	8.261, 8.262 8.255	8.285, 8.280 8.249	8.244, 8.252 8.263
Volume/2 (Å^3)		570	563	566	562
Fe(T)-O		1.86	1.84–1.86	1.84–1.92	1.85–1.86
Fe(O)-O		1.94–2.06	1.99–2.06	2.01–2.08	2.01–2.05[b] 1.98–2.05[c]
X(O)-O		2.04–2.08	2.03–2.05	1.93–2.00	2.02–2.04

[a]Experimental bulk values.
[b]See text in FO layer.
[c]See text in mixed layer.

nuclear reactors as well as its extensive use in electronic devices, using the same methodology as the present work.[36] It is noteworthy that they found the GGA scheme to be generally adequate for both structural and magnetic properties of NFO, in contrast to the simpler local spin-density approximation (LSDA) approach. Some of the relevant lattice parameters and bond lengths are collected in Table I. We see that the small variation of lattice parameter a (Å) and its trends experimentally observed are reproduced:

NFO [8.336 (Ref. 37)] <MFO(8.375 30) <CFO [8.380 (Ref. 38)] <FO(8.398 32) <MnFO [8.515 (Ref. 39)], with a variation of only 1.0% for the FO/MFO and FO/CFO cases of current experimental study. The literature values listed correspond to bulk compounds; experimental values for thin films and nanoparticles vary up to ~0.1 Å. Experimentally observed stress-induced anisotropy between in-plane and perpendicular lattice constants shows similar variation. Concerning predicted distortions of the host spinels, the most prominent difference between CFO and MFO is the c/a ratio: 0.9992 vs 1.0018, respectively. MnFO and NFO present similar c/a values of 0.9960 and 0.9982, respectively. In general, the bispinels exhibit calculated a parameters intermediate between the parent spinels, with the exception of FO/MFO which shows a small contraction in lattice parameters relative to the separate compounds. A small shearing of the supercell is evident from the different a,b values seen in Table I. A schematic representation of the bispinel unit cell is given in Fig. 1.

The net charge/moment associated with an atomic site was calculated by volume integration of electronic density in spherical volumes of radius R_{WS} which are typically chosen consistent with empirical ionic radii, and adjusted to meet criteria of chemical intuition. Some selected values, averaged over chemically equivalent sites, are presented in Table II. Note that the sum of R_{WS} charges over a unit cell is not precisely zero, due to overlap of cation and anion integration volumes. First, let us compare net charges of bulk compounds: recall that in the inverse spinel FO Fe(T) has formal ionicity +3, while the average at O sites is +2.5; however, formal charges at cation sites are not realized for any reasonable volume integration radius. Even for radii as small as

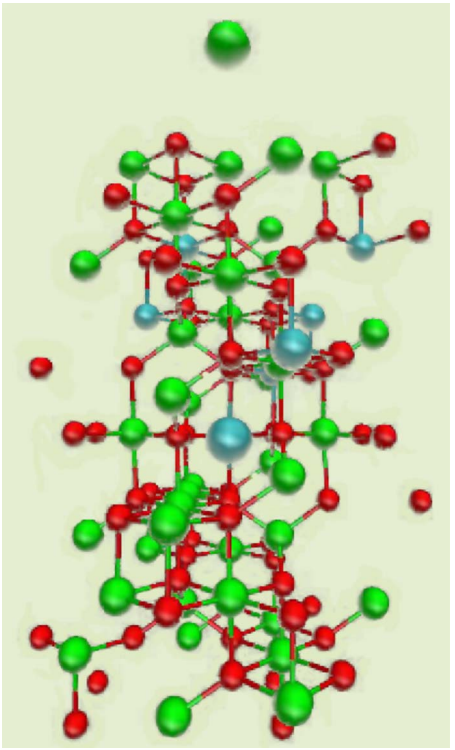

FIG. 1. (Color online) Structure of for FO/XFO bispinel multilayer unit cell, with c-axis vertical. Color code: green—Fe; blue—Mg, Mn, Co, and Ni; and red—oxygen.

TABLE II. R_{WS}-volume integrated site charges (e) and magnetic moments (μ_B) in bulk and multilayer spinels. Range of values is given, where variable over sites. Interface energies Δ (meV/Å^2, see text) are given for bispinels.

	R_{WS} (Å)	Charge	Moment	R_{WS} (Å)	Charge	Moment
			FO			
Fe(T)	0.95	1.72	−3.75	1.2	1.63	−3.33
Fe(O)	0.95	1.59, 1.79	+3.35, +3.86	1.2	1.75	+3.47, +3.48
O	1.52	−1.46, −1.44	+0.04, +0.11	1.52	−1.42	0.10
			30.59[a]			32.00[a]
			MFO			
Fe(T)	0.95	1.71, 1.76	−3.77, −3.79			
Fe(O)	0.95	1.71, 1.76	+3.84, +3.87			
Mg(O)	0.80	1.90	±0.001, 0.003			
O	1.52	−0.57, −0.66	±0.03, +0.40			
			9.85[a]			
			CFO			
Fe(T)	0.95	1.69, 1.76	−3.72			
Fe(O)	0.95	1.69, 1.76	3,84			
Co(O)	1.00	1.31	+2.51			
O	1.52	−0.52, −0.50	+0.05, +0.11			
			23.80[a]			
		FO/MFO			FO/NFO	
Fe(T)	0.95	2.87[b] 2.78, 2.90[c]	−3.75 [b] −3.76, −3.82 [c]	1.2	1.59, 1.60[b] 1.59[c]	−3.26, −3.27 [b] −3.26, −3.27 [c]
Fe(O)	0.95	2.71, 2.80[b] 2.65, 2.85[c]	+3.62, +3.74 [b] +3.60, +3.78 [c]	1.2	1.72, 1.73[b] 1.74, 1.75[c]	3.42, 3.48[b] 3.52, 3.56[c]
M(O)	0.80	1.99	±0.001,0.003	1.2	1.57	1.27, 1.29
O	1.52	−1.48, −1.55 [b] −1.38, −1.53 [c]	+0.03, +0.12 [b] ±0.01, +0.27 [c]	1.52	−1.44, −1.45 [b] −1.44, −1.47 [c]	+0.08, +0.12 [b] +0.07, 0.11[c]
			41.94[a]			47.95[a]
Δ	617			619		
		FO/CFO			FO/MnFO	
Fe(T)	1.2	1.58, 1.60[b] 1.57, 1.58[c]	−3.25, −3.28 [b] −3.22, −3.25 [c]	1.2	1.59, 1.61[b] 1.61, 1.63[c]	−3.28, −3.30 [b] −3.24, −3.29 [c]
Fe(O)	1.2	1.71, 1.72[b] 1.73, 1.74[c]	+3.43, +3.47 [b] +3.49, +3.51 [c]	1.2	1.73, 1.74[b] 1.70, 1.72[c]	+3.38, 3.44[b] +3.30, +3.36 [c]
M(O)	1.2	1.61, 1.63	+2.30, +2.35	1.2	1.77, 1.83	+2.69, +3.18
O	1.52	−1.67	+0.09, +0.12	1.52	−1.44, −1.50 [b] −1.46, −1.54 [c]	+0.05, +0.10 [b] +0.01, +0.07 [c]
			55.54[a]			56.10[a]
Δ	616			630		

[a]Net moment per supercell.
[b]In Fe_3O_4 layer.
[c]In mixed layer.

0.8 Å for Mg in MFO one finds lesser net charge (1.90e); with R_{WS} of 0.95 Å for Fe one also finds somewhat reduced values (1.59e–1.79e in FO, 1.71e–1.76e in MFO, and 1.69e–1.76e in CFO). With 1.2 Å chosen for both Fe(O) and Fe(T) sites to best include magnetization densities one finds necessarily somewhat smaller values (1.63e–1.75e in FO). Charge neutrality of the unit cell implies that ionicity of the oxyanions is also reduced and considerably variable, ranging from −0.50e to −1.46e. The spin-only moment of 5μ_B for Fe^{3+} is typically reduced to 3.33μ_B–3.79μ_B at T sites in the bulk compounds, according to the GGA exchange-correlation model employed. O-site moments are similar, ranging over 3.47μ_B–3.87μ_B showing the considerable influence of covalency and the local chemical environment. Next, let us turn to a detailed examination of FO/XFO bispinel multilayer structures.

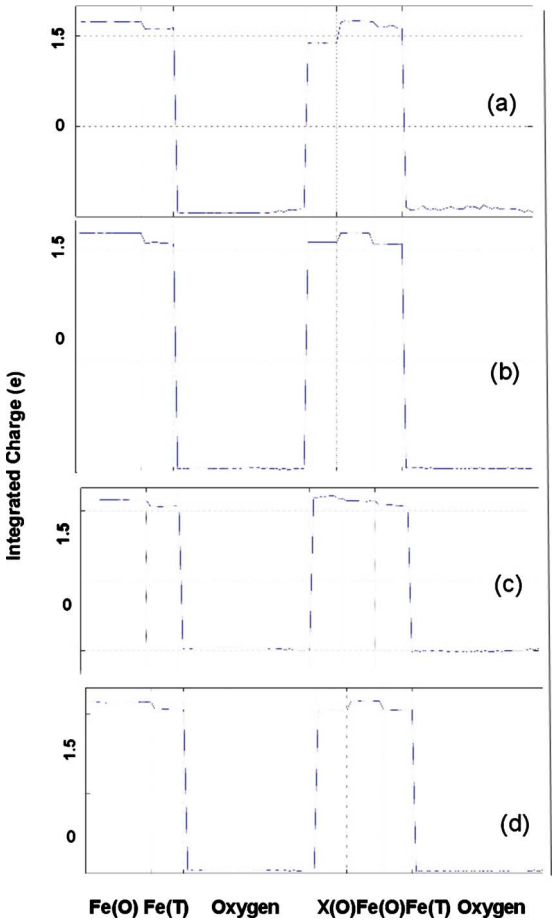

FIG. 2. (Color online) Volume-integrated charge profiles organized by site-type along the c axis: Fe(O), Fe(T), oxygen, X(O), Fe(O), Fe(T), oxygen. Within a site type, atoms are arranged by distance from top of slab. (a) FO/MFO, (b) FO/CFO, (c) FO/MnFO, and (d) FO/NFO.

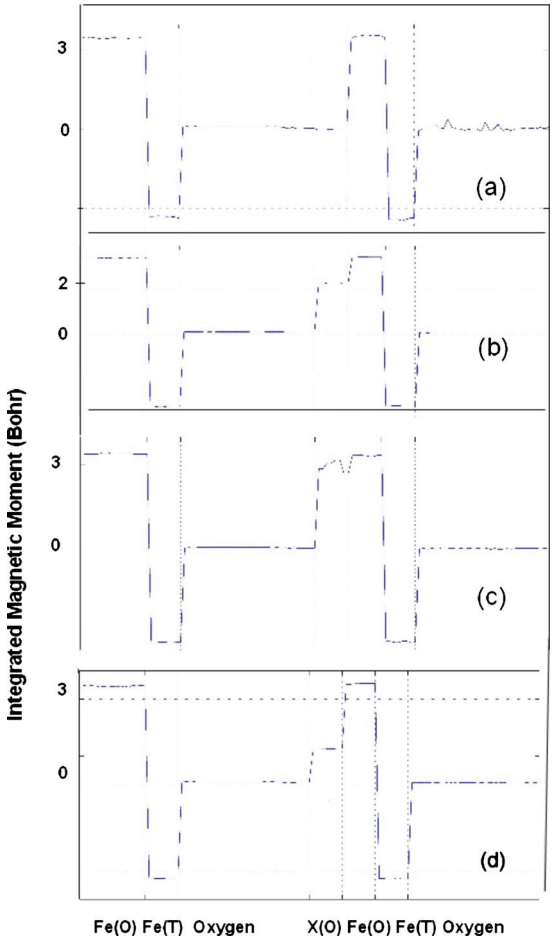

FIG. 3. (Color online) Volume-integrated magnetization profiles organized by site-type along the c-axis: Fe(O), Fe(T), oxygen, X(O), Fe(O), Fe(T), oxygen. Within a site-type, atoms are arranged by distance from top of slab. (a) FO/MFO, (b) FO/CFO, (c) FO/MnFO, and (d) FO/NFO.

1. FO/MFO

For FO/MFO, an "alloy" or "mixed spinel" model was adopted, in which Fe and Mg O-site atomic planes alternate. The objective here is to observe effects of chemical and magnetic dilution of the transition metal by the divalent diamagnetic Mg. This model was also used in the transition metal-transition metal mixed spinels discussed below. Table II reports that Fe(O) have a well-defined valency with slight, but significant differences in the FO vs MFO component slabs ($2.71e-2.80e$ in FO and $2.65e-2.85e$ in MFO with R_{WS} of 0.95 Å). A similar observation can be made for Fe(T), with $2.87e$ in FO and $2.78e-2.90e$ in MFO components. Fig. 2(a) shows the same system in a graphical representation, with R_{WS} for the cations increased to 1.2 Å, more useful for analysis of magnetization distributions. Here, the ordering is by site symmetry: O, followed by T, followed by oxygen, first for the FO slab, followed by the alloy slab. Within each section, ordering is by distance along the c axis of the supercell. With R_{WS} of 1.2 Å for cations, and 1.52 Å for oxygen, the Fe(O) net charge is found to be $\sim 1.75e$, with the oxyanion at $\sim -1.4e$. A comparison with the data of Table II is useful: aside from the obvious decrease in predicted ionicity implied by electrons swept up in the increased integration volume, we also note that in this projection of the density, T sites appear to be less ionic than O sites, contrary to analysis with smaller atomic volumes. This is sufficient to make clear that interpretations of relative changes in charge distribution are always more reliable than attempts to assign any absolute values.

Graphical analysis of volume integrated magnetization is presented in Fig. 3(a); numerical values are listed in Table II. In general one sees majority spin α on Fe(O) partially compensated by β spin on Fe(T) sites. As expected, Mg displays essentially zero magnetization, while oxygen sites show variable polarization due to covalent exchange typically of $<0.1\mu_B$. This gives a quantitative measure of the metal-ligand-metal spin coupling providing the detailed mechanism of superexchange frequently invoked to explain long-range magnetic interactions in a variety of transition metal compounds. Oxygen moments are seen to be considerably increased in the MFO slab. Magnetization is increased slightly ($<0.1\mu_B$) on Fe(T) sites within MFO, while the spread of moments increases slightly on Fe(O) sites. The net magneti-

zation of the FO/MFO supercell of $41.94\mu_B$ is slightly greater than the sum ($40.44\mu_B$) of FO and MFO calculated values.

The positive interface energy of 617 meV/Å^2 indicates that the FO/MFO bispinel is thermodynamically stable, as is found (Table II) for all compositions studied here. Partial densities of states (PDOS) are given in Fig. 4. Here and in the following, one-electron energies are given in reference to the Fermi energy $\mathbf{E}_F$. The primary features of the FO slab are as follows.

(1) As in bulk FO, the sixteen Fe(O) sites show spin α essentially fully occupied, with an occupied band width ΔE of ~ 7 eV and a clearly defined two subband structure, corresponding to the quasioctahedral t and e local symmetry. The β-spin band has small occupation, with E_F falling on the steep shoulder of the t sub-band. This is consistent with the so-called "half-metal" character of bulk FO. In the eight Fe(T) sites α spin is only slightly occupied, with a small peak at ~ -1 eV, while β spin is essentially fully occupied, with occupied ΔE of ~ 7 eV as for the O sites. The Fe(T) PDOS is nearly zero around E_F, implying that low-energy excitations, conduction and magnetic properties are largely controlled by O sites, which we may attempt to modify in the "alloy" slab.

(2) Within the MFO slab, the eight Fe(O) sites are interlaced with Mg(O) sites and continue to show spectral properties very similar to those of FO: α spin is nearly completely occupied, and β spin is nearly empty. There are some differences in detail, however; the "crystal field" peaks are somewhat broadened, and intensity is increased in the lower valence band region, indicating increased Fe-O covalency. The Fe(T) bands of either spin are also broadened, compared to FO, and a second well-defined subband appears below E_F. The near-zero PDOS around E_F is preserved, so that again, the MFO T sites play little role in transport properties.

(3) The eight Mg(O) sites present a somewhat asymmetric α- vs β-spin PDOS, due interactions with the dominant α-spin Fe(O); nevertheless, the integrated moment over the ~ 8 eV ΔE occupied band region is negligible, as expected. The region -18 to -20 eV shows interaction with the O $2s$ bands as well as with the O $2sp$ upper valence bands from -8 to 0 eV. The Mg PDOS is essentially zero around E_F as expected from its nominal divalent ionic structure and the insulating character of MgO, which is locally isostructural.

(4) The 32 oxygen sites in each slab generate very similar PDOS, characterized by an O $2sp$ band ΔE of ~ 7.5 eV and a small, but nonzero net magnetic moment. The O $2s$ bands from -18 to -20 eV are essentially nonpolarized, as expected from their lesser spatial extent. The presence of weak antibonding structures above E_F gives further evidence for the covalent Fe-O (and to a lesser extent, Mg-O) interactions.

2. FO/CFO

For FO/CFO, the effect of layering the two materials penetrates the entire FO layer with charges increased vs bulk at the interface and within the layer. According to Table II, with cation R_{WS} of 1.2 Å, the FO Fe(T) site is about $0.15e$ more ionic than the Fe(O) site, very similar to bulk magnetite,

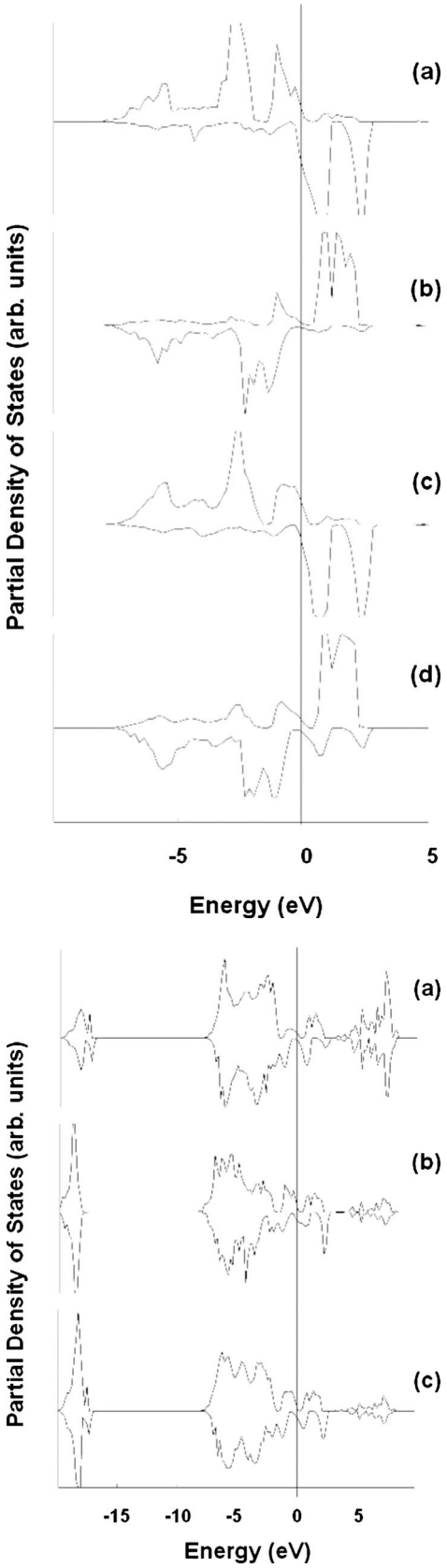

FIG. 4. Partial densities of states for FO/MFO in GGA model. (a) Fe(O), (b) Fe(T), (c) Mg(O), (d) Fe(O), (e) Fe(T), (f) oxygen in FO slab, and (g) oxygen in MFO. Positive curves are for majority spin component; negative curves represent minority spin.

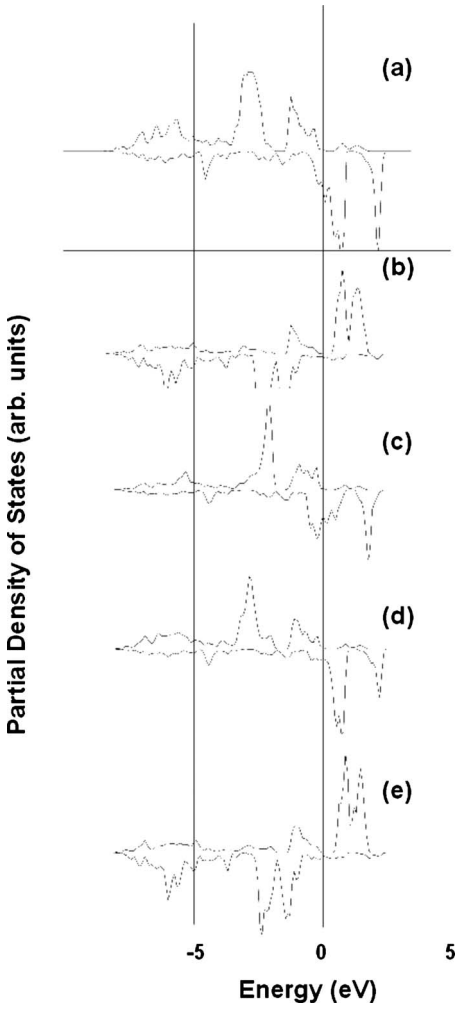

FIG. 5. Partial densities of states for FO/CFO in GGA model. (a) Fe(O), (b) Fe(T), (c) Co(O), (d) Fe(O), (e) Fe(T), (f) oxygen in FO slab, and (g) oxygen in MFO slab. Positive curves are for majority spin component; negative curves represent minority spin.

while the Co(O) site is very similar to Fe(O). Figure 2(b) shows the relations clearly. The anion ionicity of $\sim -1.5e$ is insensitive to the presence of the FO/CFO interface.

The largest magnetization change occurs on Fe(T) at the interface and within the FO layers where the magnetization increases by net amount of $0.14\mu_B$/species. The calculated magnetization of $55.54\mu_B$/cell is $1.15\mu_B$ greater than the sum of theoretical bulk FO and CFO values, see Table II and Fig. 3(b).

The FO/CFO interface energy, of 616 meV/Å^2, is essentially identical to that of FO/MFO. Turning to the densities of states, looking first at the GGA model used in structural relaxation, Fig. 5, we find that the upper valence band, of overall width 10.7 eV of which $\Delta E=8.2$ eV falls below E_F, is an intimate mixture of Fe and Co of both majority α and minority β spin, as well as lightly polarized oxygen $2sp$ composition. Resolving the PDOS into FO and CFO slab contributions, one finds the FO slab to be very similar to that of FO/MFO. The eight Co(O) sites interspersed with Fe(O) in the CFO slab show a nearly full α-spin character superficially similar to that of Fe, except for a shift of the most prominent peak to lesser binding energy, contrary to its increased atomic number and more tightly bound d electrons. Different from iron, a significant portion of the β-spin Co band falls below E_F, leading to the reduced moment seen in Table II. Both components of the multilayer are thus predicted to be metallic, with Fe minority spin peaks from FO and Co in CFO dominating at E_F. The Fe(O) β-spin states in CFO are shifted well above E_F, thus not contributing to transport properties. Alloying with Co in CFO has thus greatly modified the Fe PDOS around the Fermi energy, effectively knocking it out of conduction processes. The lower valence band, ~ 19 eV below E_F, of width 1.8 eV and primarily of oxygen $2s$ character, contains a small amount of metal character, which further contributes to the superexchange mechanism.

It is well known that density-functional theory in its various forms, including the presently used GGA, has serious shortcomings in its treatment of on-site Coulomb correlations, with serious consequences for some properties of transition metal oxides, such as the presence or absence of a gap around E_F, which is vital for a one-electron picture of low energy excitations and transport. In a subsequent section, we shall return to the PDOS, in the framework of the explicitly correlated GGA+U model. Thus, we must withhold judgment, for the moment, as to whether the CFO slab in FO/CFO is a conductor or a small gap insulator.

3. FO/MnFO

The volume integrated ionicity of O-site Mn ($1.77e-1.83e$, Table II) is greater than that of Co and Ni and comparable to that of the FO component, $1.73e-1.74e$ for Fe(O), while still less than the nearly ideally divalent Mg. The Fe(T) sites report net charges of $1.59e-1.63e$, very similar to FO/NFO (see below) and considerably less ionic than their Mg and Co counterparts. The oxyanion ionicity of FO/MnFO is also very similar to that of FO/NFO, and less than that of the other compounds. The net magnetic moment of $56.10\mu_B$ is the largest of any composite modeled, as might be expected, due to the larger Mn atomic moments ($2.69\mu_B-3.18\mu_B$). The majority spin Fe(O) moments are slightly suppressed, compared to the other systems; otherwise one would obtain an even larger total magnetization. The charge and magnetization histograms for FO/MnFO are given in Figs. 2(c) and 3(c), respectively, where one can see that the distributions differ less than for any other composite. A slight charge transfer from Mn to Fe and a slight reduction in moment (along with some irregularity) is discernable, consistent with the tabular data.

The FO/MnFO interface energy is 630 meV/Å^2, slightly larger than that of the other systems studied, an indication of a relative high degree of stability. Concerning the GGA density of states (not shown), the FO slab is very similar to that presented above for FO/MFO and FO/CFO. In the MnFO slab the Mn band features are shifted upward, to lesser binding compared to Fe, as is observed for CFO, with the dominant α-spin peak centered at ~ -2 eV. The position of these band features is thus clearly determined by chemical interactions in the slab, and not by the (rather different) atomic/ionic d-electron energies. In contrast to CFO, the β-spin Mn

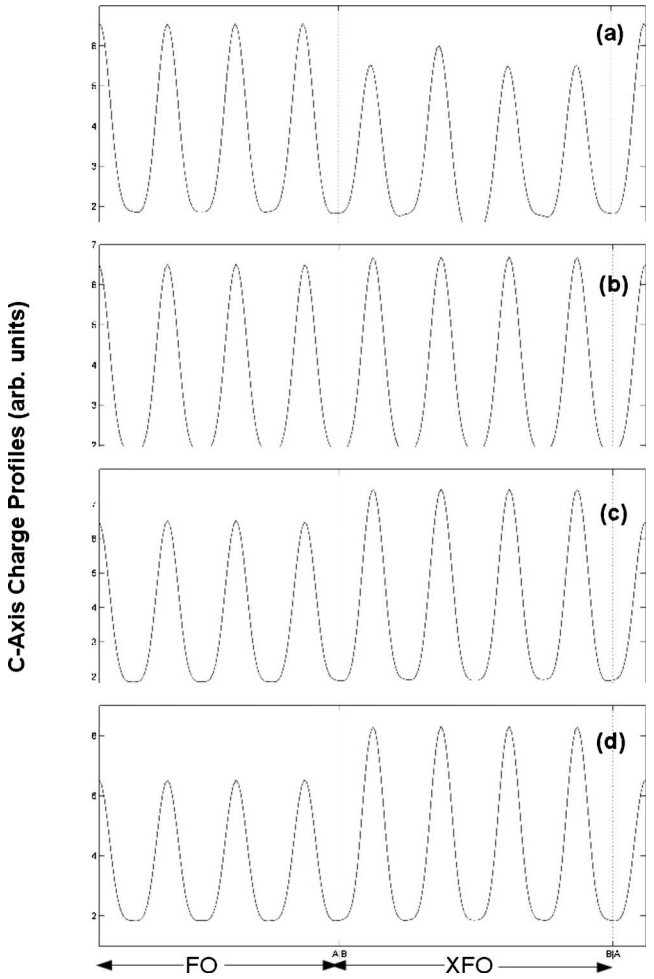

FIG. 6. Charge density profile, $\rho(z)$, integrated over the x-y plane. (a) FO/MFO, (b) FO/CFO, (c) FO/MnFO, and (d) FO/NFO.

band is nearly unoccupied, consistent with the high spin state of divalent Mn. The Fe(O)- and Fe(T)-site PDOSs in the MnFO slab are quite similar to those of FO/CFO. The c-axis charge projection [Fig. 6(c); see discussion below] reminds us that also Mn is more ionic than Fe here, the MnFO slab is comparatively electron rich, in order to compensate the higher nuclear charge of Mn. Projection of magnetization on the c axis [Fig. 7(c), see below] shows the highly symmetric ferrimagnetic configuration of the MnFO slab, with moment slightly reduced compared to Fe in FO.

4. FO/NFO

The Fe(O) and Fe(T) calculated ionic charges in FO/NFO are similar to those of FO/MnFO, and appreciably less than that of the Mg and Co composites, as is true for the oxyanion charges. The relatively low-Ni(O) ionicity of 1.57e is comparable [Fig. 2(d)] to that of Co (1.61e) in FO/CFO and with that of Fe(T) in FO/NFO. The total magnetic moment of 47.95μ_B while higher than that of the "dilute magnet" FO/MFO, is appreciably smaller than that of either Co- or Mn-based composites, primarily due to the smaller (1.27μ_B–1.29μ_B) Ni moments [Fig. 3(d)].

The FO/NFO interface energy of 619 meV/Å^2 is intermediate to that of FO/CFO and FO/MnFO. Concerning the

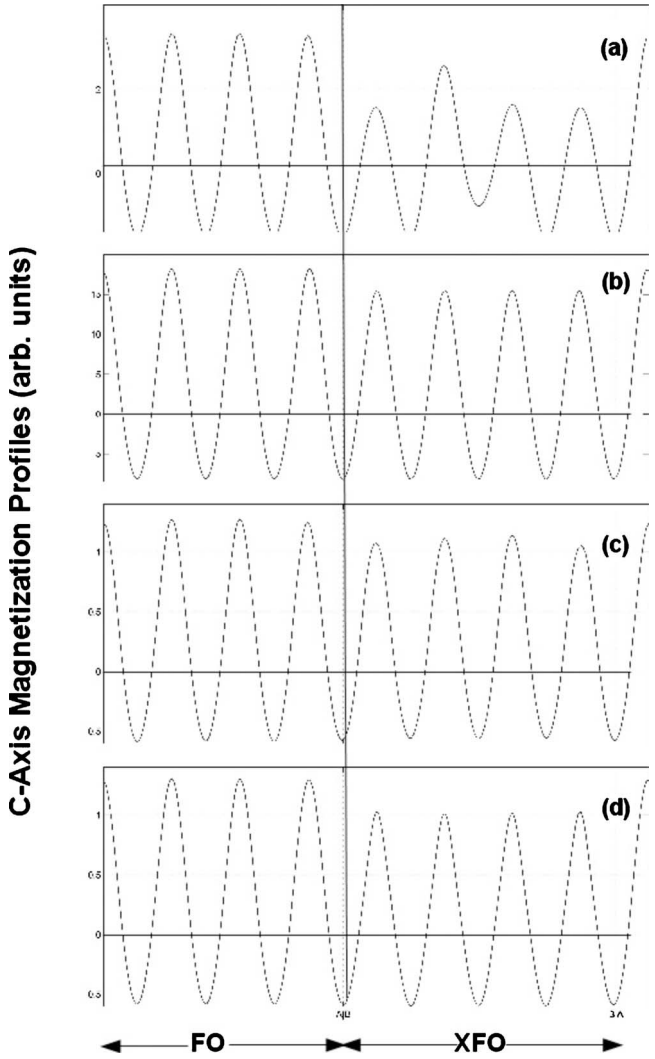

FIG. 7. Magnetization density profile, $\rho(z)$, integrated over the x-y plane. (a) FO/MFO, (b) FO/CFO, (c) FO/MnFO, and (d) FO/NFO.

densities of states (not shown), the FO PDOS structure again shows itself to be very insensitive to its companion slab; only detailed examination of atoms within 1–2 atomic layers of the interface show any real variation. This is of course consistent with the very small lattice mismatches, and the isoelectronic nature of the cation substitutions in the different composites. The Ni(O) PDOS reveal a nearly fully occupied α-spin band, with now-familiar features: $\Delta E \sim 7.5$ eV, a main peak at ~ -2 eV, and broadened structure extended up to E_F. A considerable portion of the β-spin band is occupied, with a well-defined peak at ~ -1 eV, leading to the small net magnetic moment. The Fe(O) and Fe(T) components of the NFO slab are hardly distinguishable from those of other composites.

5. Density profiles

Charge- and spin-density maps provide insight into bonding mechanisms and the pathways for magnetic interaction. Examination of contour and stereographic projections of charge density ρ_c and spin density ρ_s are very helpful in

understanding role of covalency and charge transfer in oxide materials. In the present context, axis-projected density profiles $\rho(z)=\int\rho(r)dxdy$ are especially helpful in revealing interfacial effects, and in forming some ideas about transport mechanisms. Some comparisons between the various FO/*X*FO composites (*X*=Mg, Co, Mn, and Ni) can be made by examining profiles presented in Figs. 6 and 7. As mentioned previously the (001) stacking sequence can be considered as alternating Fe_4O_8 and Fe_2 layers; however, from Figs. 6 and 7, one immediately sees that the electron density of each slab (FO and *X*FO) partitions cleanly into four layers, each of (X_6O_8) composition in accordance with Bader's definitions of topological densities.[40] Starting with the valence charge density ρ_c of FO/MFO [Fig. 6(a)] one sees that the four FO layers are highly symmetrical, with hardly any perturbation visible at the slab boundaries. Electron density in the MFO slab is appreciably lower compared to FO, with the central layers somewhat different from the boundaries. The profile for FO/CFO [Fig. 6(b)] shows a much more homogenous system, with a slightly higher density (electron accumulation) on the CFO slab. Virtually no boundary effects are visible for either slab, attesting to the excellent lattice match and the chemical similarity of Fe and Co. Both FO/MnFO and FO/NFO [Figs. 6(c) and 6(d)] show charge accumulation in the *X*FO slab; i.e., charge transfer from Fe to the substituent.

Turning now to spin densities ρ_s one again sees clean topological separation of profiles into four layers per slab, with both positive *O*-site and negative *T*-site contributions. A highly symmetric ferrimagnetic structure appears for FO in FO/MFO [Fig. 7(a)] while the MFO slab density is somewhat irregular, but overall still slightly positive, with counterbalancing $Fe_8(O)$ and $Fe_8(T)$ components. As noted earlier, the Mg(*O*) spin density is, as expected, essentially zero. The FO/CFO spin profile [Fig. 7(b)] is as highly symmetric as its charge profile; however, the lesser net spin on the $Co_8(O)$ sites leads to a reduced amplitude in the CFO slab. The profiles for FO/MnFO and FO/NFO [Figs. 7(c) and 7(d)] are qualitatively similar, showing the high symmetry associated with excellent interface matching, and the reduced moments predicted on the $X_8(O)$ substitution sites. In spintronic applications it is desirable to be able to reverse the magnetization of one slab relative to the other. This will be possible when the coercive fields of the two slabs are significantly different. While we can not predict coercive fields from the present models, we can determine the energy difference between the putative magnetic ground states just presented, and a state in which one of the slabs has its majority spin reversed. For example, the spin-flip energy for FO/CFO is calculated to be 69 meV/Å^2 or approximately 10% of the interfacial energy. This rather large coupling energy between the two slabs could be moderated by doping at the interface, to facilitate switching.

B. Correlation and spin-orbit effects

1. Hubbard-U correlation model

When the simplified GGA+*U* correlation interactions are turned on, the PDOS change in the expected significant manner: taking "magnetically diluted" FO/MFO as an example, the majority α spin band of the 16 Fe *O*-site FO region remains essentially fully occupied, but is somewhat broadened (from 7.6 to 7.9 eV) and shifted (band bottom moves from 8.0 to 9.4 eV below E_F). The relative intensity of the upper crystal field bands decreases relative to the covalently mixed Fe 3*d* and O 2*sp* lower band regions. The corresponding slightly occupied β spin band is much less affected, shifting by ~0.1 eV and continuing to display the *t* and *e* two subband structures (Fig. 8). The Fe *T*-site FO region continues to display dominant spin β character, the occupied region shifting down in energy by 0.8 eV and broadening from 6.9 to 7.7 eV. The largely unoccupied α band also broadens, from 1.7 to 3.9 eV. The Fe of the CFO segment consist of 8 *O*-site α-dominant spins followed by 8 β-dominant *T*-site spins; the occupied region increases from ~7.6 eV (GGA) to 8.6 eV (GGA+*U*); the unoccupied band regions are characterized by sharply defined *t* and *e* crystal field peaks (Fig. 9).

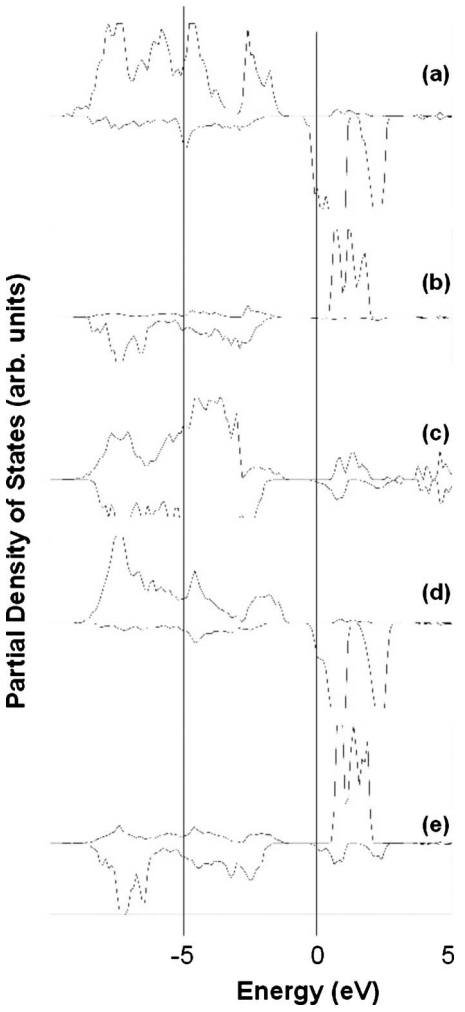

FIG. 8. Partial densities of states for FO/MFO in GGA+U model. (a) Fe(*O*), (b) Fe(*T*), (c) Mg(*O*), (d) Fe(*O*), and (e) Fe(*T*) in MFO slab. Positive curves are for majority spin component; negative curves represent minority spin.

Explicit *d*-electron correlation effects (due to *U*) on the effective moment and charge can be seen by examining the

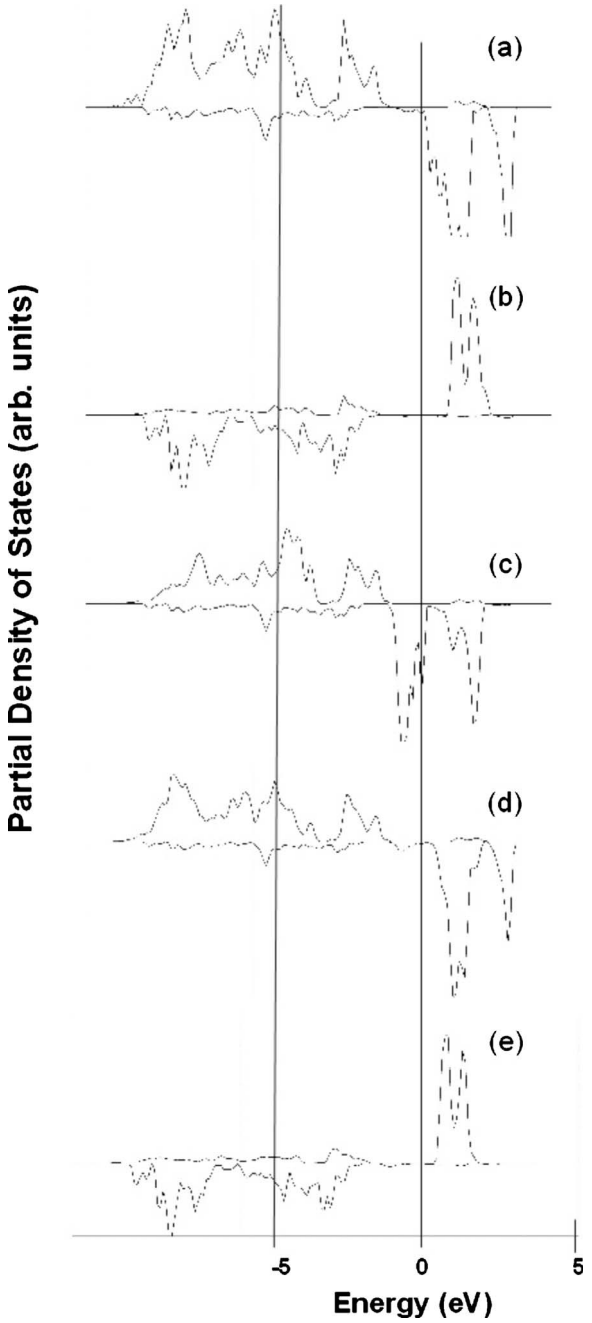

FIG. 9. Partial densities of states for FO/CFO in GGA+U model. (a) Fe(O), (b) Fe(T), (c) Co(O), (d) Fe(O), and (e) Fe(T) in MFO slab. Positive curves are for majority spin component; negative curves represent minority spin.

R_{WS} volume integrations. Using the mixed magnet FO/CFO system, we find that the application of an undifferentiated $U=4$ eV to both Fe and Co sites results in an *increase* in the Fe moments and a *decrease* in the Co moments. In FO, average T-site moments increase from $3.45\mu_B$ to $4.15\mu_B$, O site from $3.27\mu_B$ to $3.94\mu_B$, while in CFO the average of Co(O) moments changes from $2.28\mu_B$ to $1.71\mu_B$, Fe(T) moments change from $3.49\mu_B$ to $4.09\mu_B$, and Fe(O) change from $3.23\mu_B$ to $3.92\mu_B$. These magnetization changes are accompanied by charge transfers: in general Fe become more positive by $0.3e-0.4e$, while Co are partially reduced, gaining $0.9e$. Of course, these values could be shifted by use of different U values for the two magnetic cations; however, there are no experimental data to give guidance for such a multilayer system. These results do, however, give a measure of the importance of d-electron correlations on the multilayer magnetization and its distribution. The net magnetization of the 112 atom FO/CFO cell is hardly changed: $56.21\mu_B$ (GGA) vs $56.81\mu_B$ (GGA+U).

2. Direction (hkl) of spin

Spin-orbit (SO) effects were calculated post-SCF; i.e., electronic relaxation was carried out with a specified orientation of the magnetic spin axis, without permitting ionic motion. Thus, magnetoelastic effects were explicitly excluded. The overall SO energy lowering with $S(hkl)$ in an arbitrary orientation is 100–400 meV (FO/CFO, 350; FO/MFO, 166 meV) The smallest shift is observed for the magnesium-iron composite with 32 transition metal atoms/cell in FO/MFO versus 48 in FO/CFO as would be expected. Perhaps due to the small slab thickness (1 unit cell for each component) the (hkl) orientation dependence of energy is found to be small; the (001) axis is favored by only 2 meV in FO/CFO, while (001), (110), and (111) axes are found to be equivalent in FO/MFO, with a 3 meV penalty for alignment parallel to (100). The calculated magnetic anisotropy of MnFO and NFO is ~ 1 meV, which is the order of computational error.

C. Experimental results

Magnetic hysteresis loops of the Fe_3O_4, $MgFe_2O_4$, and $CoFe_2O_4$ single layers are shown in Fig. 10(a), and those of the FO/MFO and FO/CFO bilayers in Fig. 10(b). Given in Table III are their corresponding magnetization values per area (M_s) with an accuracy of $\pm 10\%$ due to error in estimating sample area. For better comparison, these single layers are of the same thickness and synthesized using the same deposition conditions as in the bilayers. M_s of the single layer $CoFe_2O_4$ is much lower than the calculated value, which is possibly due to the magnetostriction imposed by the misfit strain from the substrate.[33] The measured M_s of the FO/MFO bilayer is 4.7×10^{-4} emu/cm^2, while the estimated value based on the sum of M_s of the Fe_3O_4 and $MgFe_2O_4$ layers is 3.9×10^{-4} emu/cm^2. This experimentally measured increase in M_s for the FO/MFO bilayer is consistent with the calculations reported here for multilayers. Similarly, for the FO/CFO bilayer, the measured M_s (5.4×10^{-4} emu/cm^2) is larger than the sum of M_s of the Fe_3O_4 and $CoFe_2O_4$ layers (4.4×10^{-4} emu/cm^2). It is also noted that the measurements reveal a larger magnitude of increase in M_s than the calculations do. As the experimental bilayers are of larger dimension compared to the supercell constructed for modeling, the additional increase is arguably attributed to the magnetostriction effect from the $CoFe_2O_4$ and Fe_3O_4 layers, which is thickness dependent.[41]

V. CONCLUSIONS

Multilayer bispinel structures, with one component being magnetite, have been modeled to investigate the origin and

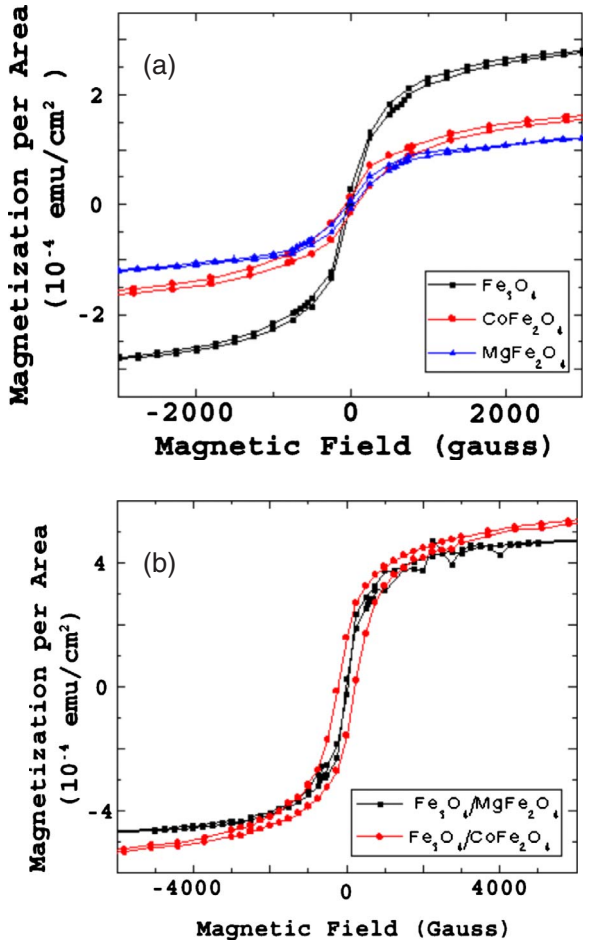

FIG. 10. (Color online) Magnetic hysteresis loops of (a) Fe_3O_4, $MgFe_2O_4$ and $CoFe_2O_4$ single layers and (b) of $Fe_3O_4/MgFe_2O_4$ and $Fe_3O_4/CoFe_2O_4$ bilayers grown epitaxially on MgO(001).

range of modifications of magnetization which can be achieved by cation substitution and distribution. Bispinel films of thickness ~20 Å were modeled by a DFT periodic supercell method, representing the lower limit of ordered experimental films produced by sputtering or evaporation. With a fixed number of lattice sites, the chemical and magnetic effects of transition metal substitutions were investigated.

A particular (001) interface deemed attractive from the point of view of metal-oxygen coordination was found to be stable (~620 meV/Å^2), with small lattice distortions (~1%) predicted well within the range of attainable epitaxial film growth parameters. Effective ionic charges and magnetic moments were determined by spherical-volume integrations; details of electronic distributions were elucidated by means of one-dimensional density profiles. It was found that "doping" of the bispinel supercell by substitution of the transition metal sites produces notable cation charge transfers and magnetization modulation. Magnetic moments at the FO/*X*FO interface are found to differ slightly from those of the slab interiors much as expected. Magnetization measurements on FO/MFO and FO/CFO bilayers show an increase, compared to single composition films, in qualitative agreement with multilayer theory. We speculate that the enhanced magnetization found in the thicker experimental films is partially due to magnetostriction imposed by the misfit strain from the substrate.

Explicit *d*-electron correlation effects were studied using the GGA+*U* model. Band shifts and gap modulation similar to that found for chemically similar bulk compounds were found. Viewed as a tunable parameter, *U* is seen to be capable of significantly modifying the density of states around E_F, and hence transport properties. The energy required to reverse the spin of the CFO slab with respect to FO in FO/CFO was calculated as 69 meV/Å^2, about 10% of the interfacial energy. In the rather thin slabs modeled here, spin-orbit coupling was found to provide only a weak contribution to the magnetic anisotropy, on the order of 3 meV/cell or less, depending upon composition.

TABLE III. Saturation magnetization values per area (M_s) for the single layer Fe_3O_4, $MgFe_2O_4$, and $CoFe_2O_4$ thin films, and, the FO/MFO and FO/CFO bilayers. These values have an accuracy of ±10% due to error from sample area estimation.

	Saturation magnetization per area M_s (emu/cm^2)
Fe_3O_4 single layer	2.8×10^{-4}
$MgFe_2O_4$ single layer	1.1×10^{-4}
$CoFe_2O_4$ single layer	1.6×10^{-4}
$Fe_3O_4/MgFe_2O_4$ bilayer	4.7×10^{-4}
$Fe_3O_4/CoFe_2O_4$ bilayer	5.4×10^{-4}

ACKNOWLEDGMENTS

This work was supported by the MRSEC program of the National Science Foundation (Grant No. DMR-0520513) at the Materials Research Center of Northwestern University. The materials synthesis work was further supported by the NSF-MRSEC program under Grants No. DMR-0076097 and No. DMR-0511523. The MPMS magnetometry measurements were performed at the Center for Nanoscale Materials at Argonne National Laboratory.

[1] N. A. Spaldin and M. Fiebig, Science **309**, 391 (2005).
[2] Y. Suzuki, Annu. Rev. Mater. Res. **31**, 265 (2001).
[3] U. Lüders, M. Bibes, K. Bouzenhouane, E. Jacquet, J.-P. Contour, S. Fusil, J.-F. Bobo, J. Fontcuberta, A. Barthélémy, and A. Fert, Appl. Phys. Lett. **88**, 082505 (2006).
[4] A. V. Ramos, J.-B. Moussy, M.-J. Guittet, M. Gautier-Soyer, C. Gatel, P. Bayle-Guillemaud, B. Warot-Fonrose, and E. Snoeck, Phys. Rev. B **75**, 224421 (2007).
[5] P. Seneor, A. Fert, J.-L. Maurice, F. Montaigne, F. Petroff, and A. Vaurès, Appl. Phys. Lett. **74**, 4017 (1999).

[6] N. Viart, R. S. Hassan, C. Mény, P. Panissod, C. Ulhaq-Bouillet, J. L. Loison, G. Versini, F. Huber, and G. Pourroy, Appl. Phys. Lett. **86**, 192514 (2005).
[7] B. B. Nelson-Cheeseman, R. V. Chopdekar, J. S. Bettinger, E. Arenholz, and Y. Suzuki, J. Appl. Phys. **103**, 07B524 (2008).
[8] Y. Suzuki, R. B. van Dover, E. M. Gyorgy, J. M. Phillips, and R. J. Felder, Phys. Rev. B **53**, 14016 (1996).
[9] M. Sohma, K. Kawaguchi, Y. Oosawa, T. Manago, and H. Miyajima, J. Magn. Magn. Mater. **198-199**, 294 (1999).
[10] A. V. Ramos, S. Matzen, J.-B. Moussy, F. Ott, and M. Viret, Phys. Rev. B **79**, 014401 (2009).
[11] A. V. Ramos, M.-J. Guittet, J.-B. Moussy, R. Mattana, C. Deranlot, F. Petroff, and C. Gatel, Appl. Phys. Lett. **91**, 122107 (2007).
[12] J.-B. Moussy, S. Gota, A. Bataille, M.-J. Guittet, M. Gautier-Soyer, F. Delille, B. Dieny, F. Ott, T. D. Doan, P. Warin, P. Bayle-Guillemaud, C. Gatel, and E. Snoeck, Phys. Rev. B **70**, 174448 (2004).
[13] D. T. Margulies, F. T. Parker, M. L. Rudee, F. E. Spada, J. N. Chapman, P. R. Aitchison, and A. E. Berkowitz, Phys. Rev. Lett. **79**, 5162 (1997).
[14] W. Eerenstein, T. T. M. Palstra, S. S. Saxena, and T. Hibma, Phys. Rev. Lett. **88**, 247204 (2002).
[15] A. V. Ramos, J.-B. Moussy, M.-J. Guittet, A. M. Bataille, M. Gautier-Soyer, M. Viret, C. Gatel, P. Bayle-Guillemaud, and E. Snoeck, J. Appl. Phys. **100**, 103902 (2006).
[16] B. A. Calhoun, Phys. Rev. **94**, 1577 (1954).
[17] Z. Zhang and S. Satpathy, Phys. Rev. B **44**, 13319 (1991); M. Fonin, R. Pentcheva, Yu. S. Dedkov, M. Sperlich, D. V. Vyalikh, M. Scheffler, U. Rüdiger, and G. Güntherodt, *ibid.* **72**, 104436 (2005).
[18] T. A. S. Ferreira, J. C. Waerenborgh, M. H. R. M. Mendonça, M. R. Nunes, and F. M. Costa, Solid State Sci. **5**, 383 (2003).
[19] D. Levy, V. Diella, M. Dapiaggi, A. Sani, M. Gemmi, and A. Pavese, Phys. Chem. Miner. **31**, 122 (2004).
[20] S. M. Antao, I. Hassan, and J. B. Parise, Am. Mineral. **90**, 219 (2005).
[21] J. M. Hastings and L. M. Corliss, Phys. Rev. **104**, 328 (1956).
[22] S. H. Lee, S. J. Yoon, G. J. Lee, H. S. Kim, C. H. Yo, K. Ahn, D. H. Lee, and K. H. Kim, Mater. Chem. Phys. **61**, 147 (1999).
[23] G. Kresse and J. Hafner, Phys. Rev. B **47**, 558 (1993).
[24] G. Kresse and J. Hafner, Phys. Rev. B **49**, 14251 (1994).
[25] G. Kresse and J. Furthmüller, Comput. Mater. Sci. **6**, 15 (1996).
[26] G. Kresse and D. Joubert, Phys. Rev. B **59**, 1758 (1999).
[27] H. J. Monkhorst and J. D. Pack, Phys. Rev. B **13**, 5188 (1976).
[28] S. L. Dudarev, G. A. Botton, S. Y. Savrasov, C. J. Humphreys, and A. P. Sutton, Phys. Rev. B **57**, 1505 (1998).
[29] V. N. Antonov, B. N. Harmon, and A. N. Yaresko, Phys. Rev. B **67**, 024417 (2003).
[30] J. Cheng, V. K. Lazarov, G. E. Sterbinsky, and B. W. Wessels, J. Vac. Sci. Technol. B **27**, 148 (2009).
[31] J. Cheng, G. E. Sterbinsky, and B. W. Wessels, J. Cryst. Growth **310**, 3730 (2008).
[32] G. E. Sterbinsky, J. Cheng, P. T. Chiu, B. W. Wessels, and D. J. Keavney, J. Vac. Sci. Technol. B **25**, 1389 (2007).
[33] S. Xie, J. Cheng, B. W. Wessels, and V. P. Dravid, Appl. Phys. Lett. **93**, 181901 (2008).
[34] J. Cheng, S. Xie, V. P. Dravid, and B. W. Wessels (unpublished).
[35] J. Cheng and B. W. Wessels (unpublished).
[36] H. Perron, T. Mellier, C. Domain, J. Roques, E. Simoni, R. Drot, and H. Catalette, J. Phys.: Condens. Matter **19**, 346219 (2007).
[37] S. Singhal and K. Chandra, J. Solid State Chem. **180**, 296 (2007).
[38] A. Lisfi, C. M. Williams, L. T. Nguyen, J. C. Lodder, A. Coleman, H. Corcoran, A. Johnson, P. Chang, A. Kumar, and W. Morgan, Phys. Rev. B **76**, 054405 (2007).
[39] E. Veena Gopalan, K. A. Malini, S. Saravanan, D. Sakthi Kumar, Y. Yoshida, and M. R. Anantharaman, J. Phys. D **41**, 185005 (2008).
[40] R. F. W. Bader, T. T. Nguyen-Dang, and Y. Yal, Rep. Prog. Phys. **44**, 893 (1981).
[41] A. Lisfi and C. M. Williams, J. Appl. Phys. **93**, 8143 (2003).